frontiers | Frontiers in Environmental Science

TYPE Original Research
PUBLISHED 17 June 2024
DOI 10.3389/fenvs.2024.1393609

OPEN ACCESS

EDITED BY
Weichun Yang,
Central South University, China

REVIEWED BY
Ying-heng Fei,
Guangzhou University, China
Qi Wang,
Zhejiang Gongshang University, China

*CORRESPONDENCE
Jiyan Shi,
shijiyan@zju.edu.cn

RECEIVED 29 February 2024
ACCEPTED 09 May 2024
PUBLISHED 17 June 2024

CITATION
Pan S, Tong J, Luo Y, Pang J, Zhang H, Wang J and Shi J (2024), Synergy of carboxymethyl cellulose stabilized nanoscale zero-valent iron and *Penicillium oxalicum* SL2 to remediate Cr(VI) contaminated site soil.
Front. Environ. Sci. 12:1393609.
doi: 10.3389/fenvs.2024.1393609

Synergy of carboxymethyl cellulose stabilized nanoscale zero-valent iron and *Penicillium oxalicum* SL2 to remediate Cr(VI) contaminated site soil

Siyi Pan, Jianhao Tong, Yating Luo, Jingli Pang, Haonan Zhang, Jing Wang and Jiyan Shi*

Department of Environmental Engineering, College of Environmental and Resource Science, Zhejiang University, Hangzhou, China

Nano zero-valent iron (nZVI) acting as a high-cost disposable material in soil Cr(VI) remediation faces significant challenges due to its easily oxidizable nature and biological toxicity. In addressing this issue, the present study undertook the synthesis of a series of modified nZVI and combined the selected material with Cr(VI)-resistant filamentous fungus *Penicillium oxalicum* SL2 for real-site chromium pollution remediation. Adsorption experiments demonstrated that the inclusion of carboxymethyl cellulose (CMC) significantly enhanced the adsorption capacity of nZVI for Cr(VI) by 19.3% (from 73.25 to 87.4 mg/L), surpassing both biochar (37.42 mg/L) and bentonite modified nZVI (48.03 mg/L). Characterization results validated the successful synthesis of the nano composite material. Besides, oxidative stress analysis explained the unique detoxification effects of CMC on SL2, acting as a free radical scavenger and isolating layer. In real-sites soil remediation experiments, a low dosage (0.4% w/w) of nZVI/CMC@SL2 (CMC modified nZVI combined with SL2) exhibited an impressive reduction of over 99.5% in TCLP-Cr(VI) and completely transformed 18% of unstable Cr to stable forms. Notably, nZVI/CMC demonstrated its capability to facilitate SL2 colonization in highly contaminated soil and modulate the microbial community structure, enriching chromium-removing microorganisms. In summary, the synergistic system of nZVI/CMC@SL2 merges as a cost-effective and efficient approach for Cr(VI) reduction, providing meaningful insights for its application in the remediating contaminated site soils.

KEYWORDS

nZVI stabilization, carboxymethyl cellulose, Cr(VI) reduction, soil microcommunity, *Penicillium oxalicum* SL2

1 Introduction

The extensive use of chromium in industrial processes, such as electroplating, chromate production, and leather tanning (Ma et al., 2024), due to its excellent corrosion resistance and metallic luster, has resulted in its widespread release into the soil. China's 2014 nationwide soil pollution survey revealed a 1.1% excess of Cr pollution beyond national standards, with particularly severe cases in industrial zones. Recognized as a class "A" carcinogen by the United States Environmental Protection Agency (EPA) (Chen et al.,

2020) hexavalent chromium poses severe health risks through long-term exposure and food chain transmission which will cause great harm to human health and cause various diseases (Fu et al., 2023). Therefore, the urgent remediation of Cr(VI) contaminated site soil is imperative.

The main remediation method involves reducing Cr(VI) to Cr(III) (Du et al., 2023; Wang et al., 2024). Recently, because of its high reactivity and reduction capability, nano zero-valent iron (nZVI) has gained widespread use in research focusing on the remediation of Cr(VI) contaminated soil (Yang et al., 2021). However, its application potential is greatly hindered by challenges such as aggregation (Phenrat et al., 2007) and biotoxicity (Auffan et al., 2008; Ye et al., 2021). To address these issues, numerous studies have been conducted based on the surface modification of nZVI such as biochar (Su et al., 2016), chitosan (Liu et al., 2010), hydrophobic stabilizers such as carboxymethyl cellulose (CMC) (Raychoudhury et al., 2012), poly acrylic acid (Laumann et al., 2014) or starch (Wang et al., 2014). These materials can impede the gathering and oxidation of nZVI (Ambika et al., 2016), mitigate its biotoxicity (Chen et al., 2012) and enhance particle mobility in the soil (Chekli et al., 2016). However, the application dosages of these materials were often relatively high (Supplementary Table S1), leading to elevated remediation costs and potential alterations to the original physicochemical properties of the soil. Therefore, the identification of a low-dosage, efficient, and environmentally friendly remediation strategy is of paramount importance.

Beyond chemical remediation approaches, microbial remediation, regarded as an environmentally sustainable and economically feasible method for soil contamination control is extensively researched. Certain bacteria, including QY-1, extremely thermophilic bacterium *(Caldicellulosiruptor saccharolyticus)*, *Shewanella oneidensis* MR-1 as well as sulfate-reducing bacteria (SRB) and iron reducing bacteria (IRB) (Peng et al., 2015; Bai et al., 2018; Hou et al., 2020; Ma et al., 2021; Lin et al., 2022) exhibited ability of Cr(VI) reduction. Bacteria can mitigate the toxicity of heavy metals through various mechanisms such as enzymatic detoxification and intracellular isolation (Bruins et al., 2000), *etc.* There are also studies that amalgamate bacteria with nZVI to address chromium contamination (Tan et al., 2020). Nevertheless, their tolerance to Cr(VI) are relatively lower, such as *Arthrobacter* sp., *Bacillus* sp. and *Streptomyces* sp. (Megharaj et al., 2003; Elangovan et al., 2006; Morales et al., 2007) (Minimum Inhibitory Concentration range, MIC, range from 80 to 500 mg/L), the survival and remediation capabilities in actual highly contaminated site soil remain ambiguous. Contaminated site soil, characterized by diverse and elevated heavy metal concentrations (Wu et al., 2018; Sun et al., 2022) and limited organic matter, imposes constraints on microbial growth, underscoring the critical importance of identifying suitable microorganisms.

Fungi, despite demonstrating high tolerance to heavy metals and thriving in low-nutrient environments (Chen et al., 2020), have received comparatively less attention in remediation studies. *Penicillium oxalicum* SL2, a filamentous fungus with high resistance to Cr(VI) (MIC greater than 1,000 mg/L Cr(VI)), was isolated in our antecedent study (Long et al., 2018), it could grow rapidly and completely remove 96.1 mg/L Cr(VI) in electroplating wastewater after inoculation for 96 h. Strain SL2 produced acidic metabolites such as LMWOAs playing important role in the mobilization of chromium and improving bioleaching (Long et al., 2023). Its mechanisms for heavy metal pollution abatement encompass the production of small organic acids, extracellular absorption, bioprecipitation, and transmembrane transport (Tong et al., 2023). Moreover, SL2 exhibited marked iron precipitate and Fe(II) regeneration capabilities, rendering its amalgamation with nZVI a promising avenue for remediation.

To the best of our knowledge, there is currently no study on the combination of nZVI/CMC and anti-chromium fungus SL2 for the remediation of high Cr(VI) polluted sites soil (Cr(VI) ranging from 348 to 1,305 mg/kg) (Li et al., 2023). Moreover, previous studies often simulated pollution with lower Cr(VI) concentrations (Supplementary Table S1), significantly differing from the complex conditions found in real contaminated soils. Hence, the overall objective of this study was to demonstrate the effect and practicability of the integrate remediation of Cr(VI) polluted site soil by using the stabilized nZVI with SL2. Consequently, this study is specifically structured as follows: (1) synthesize various stabilized nZVI composites and determine their efficacy in removing Cr(VI) in liquid; (2) investigate the biocompatibility of stabilized nZVI with SL2 for Cr(VI) removal from aqueous solutions and determinate the optimal combination; (3) explore the detoxification effect and immobilization of Cr(VI) in soil by the developed composite system consisting of nZVI/CMC and microorganism and elucidating their potential mechanisms; (4) evaluate the impact of these materials on soil microecology. This study aims to provide a scientific basis and technological support for the practical application of nZVI/CMC@SL2 in the remediation of Cr(VI) contaminated site soil.

2 Materials and methods

2.1 Preparation of stabilized nZVI

The sample was prepared by sieving pine powder through a 100-mesh, washed with deionized water to remove impurities, and subsequently dried. Under the protection of nitrogen gas, it underwent thermal decomposition at a heating rate of 10°C/min until reaching 600°C for a duration of 2 h, resulting in the sample referred to as C. A solution containing 5.40 g $FeCl_3{\cdot}H_2O$ dissolved in 100 mL oxygen-free water with 30% anhydrous ethanol was prepared. Different loading materials and concentrations of nano zero-valent iron (nZVI) were synthesized by adding 1% carboxymethyl cellulose (CMC), varying quantities of biochar or bentonite. The solute mixture was thoroughly mixed by shaking at room temperature and at a speed of 150 r/min for 24 h. Subsequently, under a nitrogen atmosphere, sodium borohydride ($NaBH_4$) weighing 3.04 g was slowly added dropwise into the above mixture to form nZVI stabilized by CMC, biochar or bentonite (Supplementary Text S1 and Figure S1), named as nZVI/CMC, nZVI/C, nZVI/B, respectively.

2.2 Adsorption experiments and material characterization

To assess the removal efficiency of stabilized nZVI for Cr(VI) in aqueous solution, a concentration of 2 g/L of the aforementioned material was added to a solution containing Cr(VI) with an initial concentration of 200 mg/L. The reaction was conducted in a reactor operating at a rotation speed of 150 rpm and a temperature of 25°C for a duration of 72 h. Supernatant was regularly collected and

filtered through a 0.22 μm filter. The concentration of Cr(VI) in the filtrate was determined by employing the diphenyl-carbohydrazide spectrophotometric method. Subsequently, several stable materials with the best effect were selected to establish isothermal adsorption experiments with initial concentration gradients of 10, 20, 50, 100, 200, 400, and 800 mg/L for Cr(VI). Various kinetic models, including the pseudo-first-order model, pseudo-second-order model, Avrami model and intraparticle diffusion model were employed to fit the adsorption process of Cr(VI), along with adsorption isotherm models such as Langmuir, Freundlich and Sips models.

The microstructure of synthesized materials above was imaged by scanning electron microscopy (SEM, Zeiss Sigma500). Also, the products were analyzed by X-ray diffraction (XRD, D8 Advance, Bruker, U.S.A) and data were collected the 2θ range from 10 to 90°. The functional groups on the surface of the materials were characterized by Fourier Transform Infrared Spectroscopy (FTIR, Thermo Scientific Nicolet iS20). In addition, the species of Cr and Fe on the surface of reaction products were analyzed by X-ray photoelectron spectroscopy (XPS, Escalab 250Xi, UK).

2.3 Metabolic activity of SL2 suffering from nZVIs and Cr(VI)

To assess the oxidative stress response of SL2 to stable nZVI, 1% spore SL2 suspension (10^7 CFU/mL) and 1 g/L different materials (nZVI/B was not measured because of the poor growth of SL2) were introduced into Cr(VI) solution. The mixture was incubated in a shaker at 30°C and 150 rpm for 2 days. After centrifugation, the collected bacterial slurry was analyzed for intracellular ATP, reactive oxygen species (ROS), and glutathione (GSH) levels (Supplementary Text S2) as indicators of the oxidative stress reaction.

2.4 Remediation of site soil by nZVI/CMC@SL2

2.4.1 Soil preparation and experimental design

Cr(VI) polluted soil samples were collected from a chromium slag dump site in Inner Mongolia (NM), and an electroplating contamination site in Zhangjiakou, Hebei Province (soil sample with higher and lower Cr(VI) pollution was named ZH and ZL respectively), China. After removing larger impurities, the soil was sieved through a 10-mesh screen, thoroughly mixed, and air-dried, referred to as NM, ZH and ZL, respectively. Soil heavy metal concentration and physicochemical characteristics were shown in Supplementary Tables S2, S3. Candidate nZVI/CMC, exhibiting optimal performance, was chosen for soil remediation. 20 g contaminated soil was treated with a 0.4% (w/w) nZVI/CMC addition, 10^7 CFU/g soil of SL2, and deionized water to maintain a 25% moisture level, 25°C. Five treatments were set for each soil sample, carried out in triplicate: (1) Control Check; (2) sterile potato dextrose liquid medium (1:4; PDL:H_2O; v/v); (3) PDL + SL2; (4) nZVI/CMC; (5) PDL + nZVI/CMC@SL2. The soil and additives were thoroughly mixed. Samples were collected on days 0, 3, 7, 15, and 30 (Supplementary Figure S2).

2.4.2 Chemical stability of Cr in the soil after remediation

Analysis of five different chromium species in soil was performed using the Tessier sequential extraction method. The extraction solution was filtered through a 0.45 μm membrane and analyzed using an atomic absorption spectrometer. Additionally, total Cr(VI) in the soil was measured using an alkaline extraction method, leachable Cr(VI) using the TCLP extraction method and Fe(II) concentrations was determined using colorimetric method with 1,10-o-phenanthroline. Detailed extraction and measurement methods can be found in the Supplementary Text S3.

2.4.3 Soil microecology analysis

Fresh soil samples were collected from each pot to evaluate the soil microecology—SL2 microbial counts (Supplementary Text S4) and microbial community.

Soil genomic DNA was extracted using E.Z.N.A. Soil DNA Kit (Omega Bio-tek, Inc., United States) following the manual. Concentration and quality of the genomic DNA were checked by NanoDrop 2000 spectrophotometer (Thermo Scientific Inc., United States). The fungal ITS region and the bacterial 16S rRNA genes were amplified using the primer sets ITS1F/ITS2R and 338F/806R (Yao et al., 2017; Tang et al., 2018) respectively by PCR system (Applied Biosystems, Inc., United States). The amplicons were sequenced through the Illumina's Miseq PE300 platform (Illumina, Inc., United States). Qualified sequences were clustered into operational taxonomic units (OTUs) at a similarity threshold of 97% use Uparse (Edgar, 2013) algorithm of Vsearch (v2.7.1) software. Refer to Supplementary Text S5 for detailed analytical methods.

3 Results and discussion

3.1 Adsorption performance of different stabilized nZVI

3.1.1 Adsorption kinetics

In order to examine the correlation between contact time and the rate of reduction of Cr(VI) by different materials, kinetics investigations were performed with results presented in Figure 1. It could be noticed that Cr(VI) uptake increased within the initial 240 min, which might be attribute to the plentiful adsorption sites provided by the loading material and the reduction reaction of nZVI to Cr(VI). Nonetheless, with the gradual occupation of adsorption sites by Cr(VI), the rate of pollutant adsorption increased at a slower pace, reaching equilibrium after 500 min.

To quantitatively evaluate the kinetic process on Cr(VI) uptake by stabilized nZVI, four acknowledged models involving pseudo-first/second-order, Avrami fractional-order as well as intra-particle diffusion models were chosen to analyze the data (Dai et al., 2019; Qu et al., 2021; Qu et al., 2022), the formulas were shown below (Eqs 1-4):

$$q_t = q_e\left(1 - e^{-k_1 t}\right) \quad (1)$$

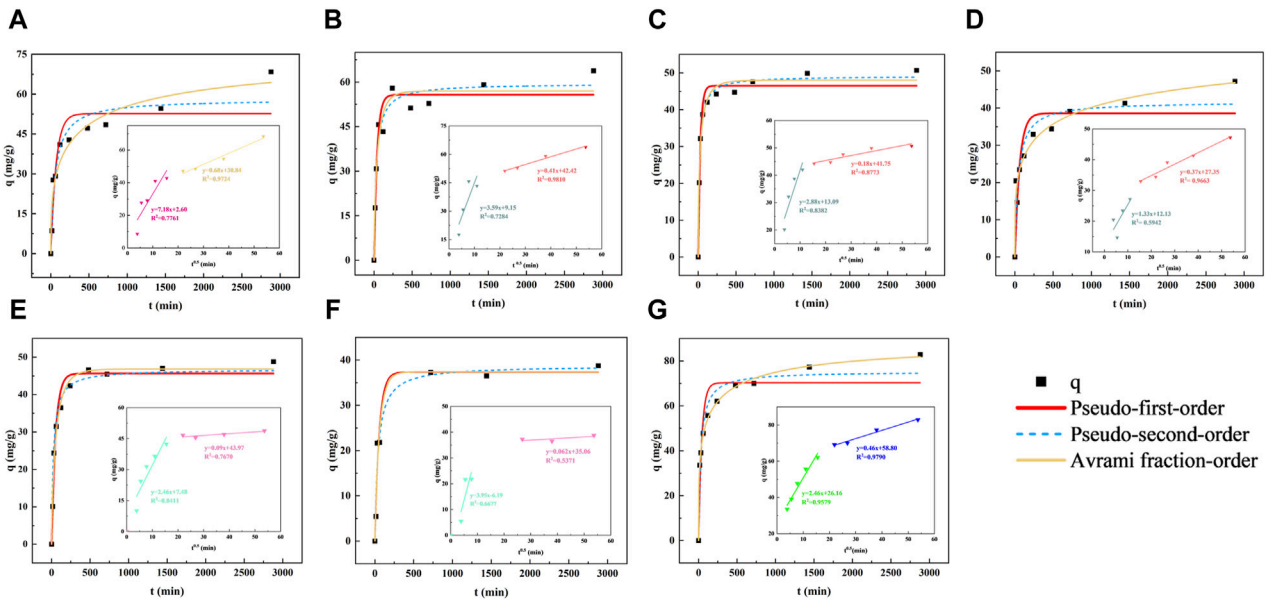

FIGURE 1
Kinetic fitting results of pseudo first-order, second-order and Avrami fractional models for Cr(VI) uptake onto stabilized nZVI (inset: intraparticle diffusion model).**(A)** nZVI; **(B–D)** nZVI/B with ratio of 1:2, 1:1, 2:1; **(E, F)** nZVI/C with ratio of 1:1, 1:2; **(G)** nZVI/CMC, T = 25°C, [Cr(VI)] = 200 mg/L, [Material dosage] = 2 g/L.

TABLE 1 Kinetic model parameters for the uptake of Cr(VI) onto stabilized nZVI.

Material	Pseudo-first-order model				Pseudo-second-order model			Avrami fractional-order model					
	q_e (mg/g)	k_1 (min^{-1})	R^2	SD	q_e (mg/g)	k_2 (g mg^{-1} min^{-1})	R^2	SD	q_e (mg/g)	k_3 (min^{-1})	n	R^2	SD
nZVI	52.65	0.0146	0.8822	3.50	58.07	0.0003	0.9297	3.47	73.25	0.0025	0.3771	0.9452	21.29
nZVI/C(1:1)	45.65	0.0192	0.9755	1.25	46.75	0.0008	0.9290	0.05	46.81	0.0166	0.7340	0.9842	1.27
nZVI/C(2:1)	37.36	0.0182	0.9599	1.98	38.77	0.0006	0.9622	2.12	37.42	0.0175	0.9116	0.9605	2.20
nZVI/B(1:1)	55.72	0.0249	0.9432	2.20	59.51	0.0005	0.9596	2.24	56.99	0.0220	0.7242	0.9505	2.57
nZVI/B(1:2)	46.51	0.0358	0.9730	1.14	49.13	0.0011	0.9904	0.80	48.03	0.0318	0.5992	0.9826	1.24
nZVI/B(2:1)	38.60	0.0162	0.8281	2.81	41.67	0.0005	0.9033	2.59	61.38	0.0012	0.2865	0.9733	25.70
nZVI/CMC	70.28	0.0244	0.8949	3.66	75.30	0.0004	0.9615	2.67	87.42	0.0076	0.3284	0.9981	3.02

$$q_t = \frac{q_e^2 k_2 t}{1 + q_e k_2 t} \quad (2)$$

$$q_t = q_e\left[1 - e^{-(k_3 t)^n}\right] \quad (3)$$

$$q_t = k_4 t^{1/2} + n \quad (4)$$

in which, q_t (mg/g) express the quantity of Cr(VI) taken up at time t; q_e (mg/g) represents the uptake of Cr(VI) adsorbed at equilibrium; kinetic constants associating with different models are k_1, k_2, k_3 and k_4. The n (mg/g) is the intercept of intraparticle diffusion model. Values of n give information about the thickness of the boundary layer, the larger intercept the greater is the boundary layer effect (Zhu et al., 2010).

Standard deviation (SD) and coefficient (R^2) were used to evaluate the suitability of each model, that was, data with lower SD and higher R^2 indicated superior applicability of the kinetic model. Detail fitting parameters were provided in Table 1. As shown, Avrami fractional-order model showed the highest R^2 value (0.9981) among these models, demonstrated to present the best appropriateness for depicting the uptake performance for Cr(VI), revealing that there were multiple kinetics during the binding processes of Cr(VI) onto nZVI/CMC (Qu et al., 2022). In addition, the R^2 (0.9615) of the pseudo-second-order is also higher than that of the pseudo-first-order model (0.8949), indicating that the rate-limiting step during the reaction was chemical adsorption involving electron exchange between adsorbent and adsorbate, rather than physical diffusion (Lyu et al., 2017). According to the intra-particle diffusion model consequences (insets of Figure 1G), two stages were involved in Cr(VI) uptake nZVI/CMC, intraparticle diffusion and external

surface binding. Besides, both of the fitting curves deviated from the base point (n = 26.16), which suggested that the intraparticle diffusion was not the rate-controlling step in Cr(VI) uptake process, but the boundary layer diffusion controlled the adsorption to some degree.

3.1.2 Adsorption isotherms

In order to investigate the effect of Cr(VI) concentration gradient on the adsorption capacity of stabilized nZVI, the interaction between them was quantitatively described using isothermal adsorption.

Three famous isotherm models including Langmuir, Freundlich and Sips models were then applied for fitting the uptake results (Eqs 5-7), which are expressed as:

$$q_e = \frac{q_{max} K_L C_e}{1 + K_L C_e} \tag{5}$$

$$q_e = K_F C_e^{1/n_F} \tag{6}$$

$$q_e = \frac{q_s (K_s C_e)^{m_s}}{1 + (K_s C_e)^{m_s}} \tag{7}$$

in which, the maximum adsorbing quantity of Cr(VI) represented by q_{max} (mg/g); K_L, K_F and n_F respectively involve the Langmuir coefficient, Freundlich coefficient and Freundlich intensity parameters; K_S and m_S are the identical Sips heterogeneity divisors.

In the Langmuir model, adsorption is considered to occur on homogeneous surface. Freundlich is an empirical model for heterogeneous systems. Sips model is a combination of Langmuir and Freundlich (Deng et al., 2020) capable of modeling both homogeneous and heterogeneous binding surfaces (Zhang et al., 2019). The results (Supplementary Figure S3; Supplementary Table S4) showed that the Sips model had the best fitting results (R^2 = 0.9302), which suggested that adsorption of Cr(VI) was a non-ideal sorption on heterogeneous (Tang et al., 2016).

In summary, the introduction of CMC significantly enhanced the removal efficiency of Cr(VI) by nZVI, for its maximum adsorption capacity of 87.42 mg/g, surpassing the performance of biochar and bentonite. Moreover, the process involved multiple kinetic mechanisms, with boundary layer diffusion identified as the primary rate-limiting step.

3.2 Characterizations of stabilized nZVI

The morphology and size of the newly prepared stabilized nZVI were characterized by scanning electron microscopy (SEM). As depicted in Figure 2A, individual particles of nZVI appeared irregularly spherical and had a diameter of approximately 50 nm. After stabilization, the nZVI was uniformly dispersed on the surface of the carriers. The CMC stabilized nZVI exhibited a reticular dendritic structure and smaller particle size, due to the significant influence of high-concentration CMC solution on the nucleation of nZVI. Throughout the nanoscale particle growth process, CMC molecules adhere to the particle surface, impeding further growth through electrostatic repulsion and steric hindrance (He and Zhao, 2007). This preservation of smaller particle sizes for nZVI results in higher reactivity in reactions. In the EDS maps, each material exhibited elevated levels of Fe element, along with characteristic elements of the loaded material, such as C, Si and Al, indicating successful loading of iron onto the material. It is noteworthy that the iron element content on the surface of nZVI/CMC (89.4%) is significantly higher than that of biochar (53.28%) and bentonite (20.21%). This characteristic enables better preservation of the nZVI properties and facilitates the reactivity towards Cr(VI) reduction. To elucidate the stabilization mechanisms and gain further insight into the various functional groups of the nanoparticles, XRD, FTIR and XPS measurements were carried out on stabilized nanoparticles. From XRD pattern, a distinctive peak corresponding to Fe (0) is observed at 2θ = 45° (Bian et al., 2021; Zhou et al., 2022). The broad peak signified the body-centered cubic (bcc) Fe (0) crystal lattice plane (110) (Lin et al., 2010) with a relatively poor crystallinity (Gong et al., 2017), providing further evidence of the presence of iron in the material in the form of zero-valent iron. The types of surface functional groups on the nanoparticles were qualitatively analyzed using FTIR spectroscopy, the characteristic broad peaks near 3,400 cm^{-1} related to the stretching vibration of -OH (Xu et al., 2020; Ji et al., 2022) were observed in all materials, potentially associated with iron hydroxides (Bian et al., 2021). Additionally, bands corresponding to C=O were identified in the range of 1,610–1,660 cm^{-1}, those acidic O-containing functional groups were reported to have a great effect on absorption and reduction of Cr(VI) (Wang K. et al., 2020). Particularly, nZVI/CMC revealed a carboxyl group (-COO) at 1,420 cm^{-1}, suggesting its role as one of the binding sites for Fe. To identify the carboxylate-metal complexation mechanism, the separation of the symmetric and asymmetric stretches [Δν = Δ(asym) − Δ(sym)] of the carboxylate group was calculated (Deng et al., 2021). In the present work, Δν was determined to be 189 cm^{-1} (1,615–1,426 cm^{-1}), proved that bidentate bridging was the primary mechanism for binding CMC molecules to Fe nanoparticles, same as the previous research (He et al., 2007; Lin et al., 2010). Simultaneously, polydentate ligands were commonly reported to possess stronger chelating affinities compared to monodentate ligands (Su and Puls, 2004), this structural characteristic enhanced the stability of nZVI/CMC, underlining the increased robustness conferred by the multidentate coordination in this complex. It is noteworthy that oxygen-containing functional groups in the materials, such as C=O, -OH and -COO may concurrently contribute electrons, thereby facilitating the reduction of Cr(VI) (Zhao et al., 2022). The implication is that the O functional groups may play a crucial role as electron transfer stations in the Cr-Fe reaction.

Further, XPS was performed for CMC-nZVI before and after Cr(VI) uptake (Figure 3). The XPS spectra before the reaction confirmed the presence of zero-valent iron in the material by a characteristic peak of Fe2p with a binding energy of 706.23 eV (Ren et al., 2018), accounting for 30.21%. Another portion of Fe, likely oxidized upon exposure to air during transportation and storage, formed Fe(II), constituting 69.79% (Yamashita and Hayes, 2008). After reaction, the peaks corresponding to Fe (0) and Fe(II) disappeared, and a characteristic satellite peak of Fe(III) emerged (Liu et al., 2020), indicating the complete oxidation of iron in the material to trivalent state. Additionally, the results of the Cr elemental partition spectra revealed that the Cr in the reaction

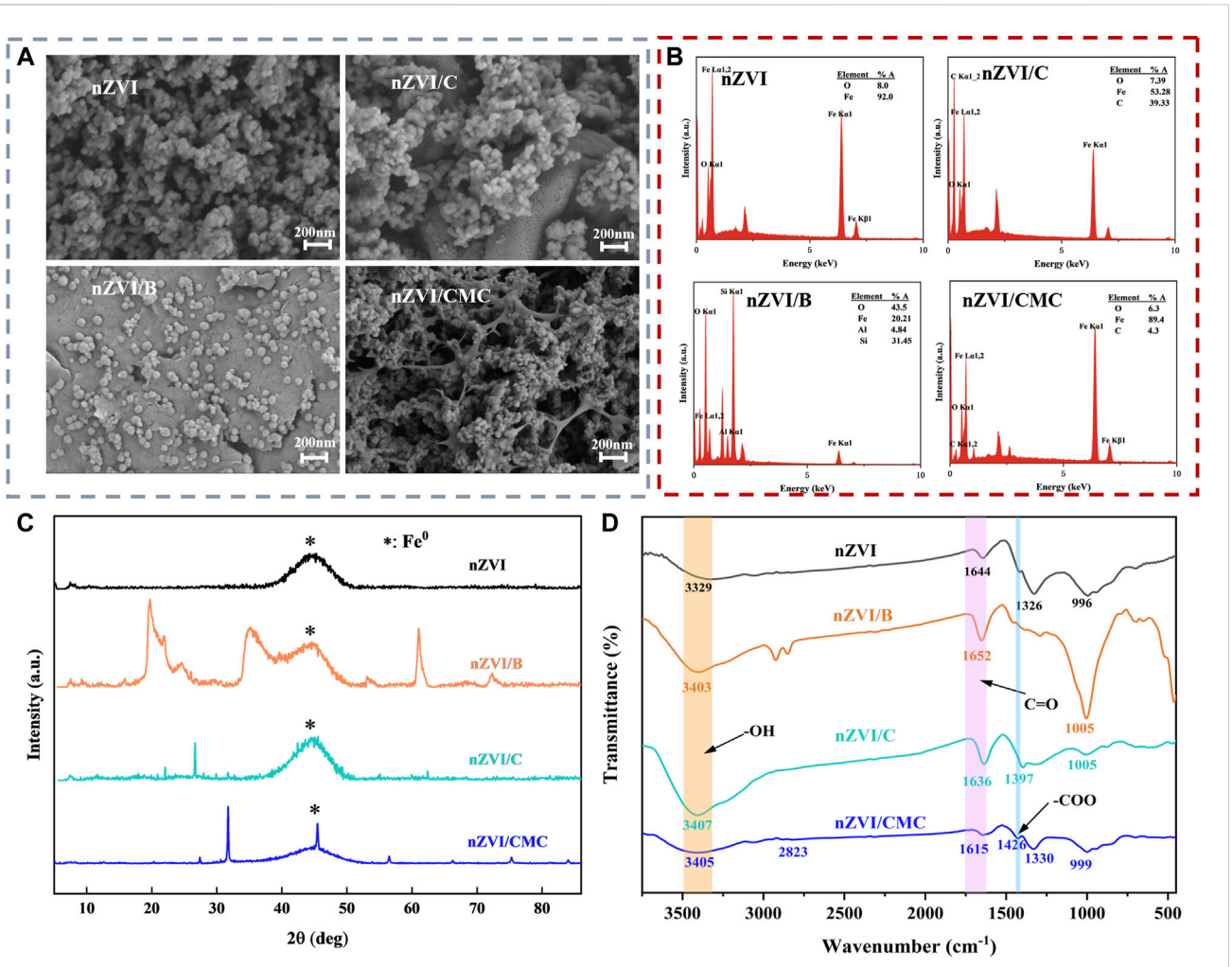

FIGURE 2
SEM **(A)**, EDS **(B)**, XRD **(C)**, FTIR **(D)** patterns of stabilized nZVI.

product existed mainly in the valence state of Cr(III), including chromium oxides and hydroxides. Therefore, both Fe (0) and Fe(II) in the material directly serve as electron donors for the reduction of Cr(VI) to Cr(III). Subsequently, these Cr(III) species co-precipitate with Fe^{3+}, forming $Cr_nFe_{1-n}(OH)_3$ (Pan et al., 2016; Ye et al., 2021). Moreover, upon contact with water, zero-valent iron generated H*, which was confirmed to be the predominant reactive species for Cr(VI) reduction (Qian et al., 2014). Besides, the abundant -OH and -C=O groups on CMC play a crucial role as electron donors for the reduction of Cr(VI) (Rajapaksha et al., 2018; Xu et al., 2019). In conclusion, the analysis confirmed that the removal of Cr(VI) by nZVI/CMC involved both adsorption and reduction processes, consistent with previous study (Fang et al., 2011).

In summary, the potential electrostatic repulsion and spatial hindrance capabilities of CMC contributed to maintaining the small size of nZVI particles, preventing its easy aggregation. Additionally, the combination of nZVI with CMC was achieved through a more stable bidentate bridging mechanism. Furthermore, it revealed that both Fe (0) and Fe(II) contributed to the reduction of Cr(VI), and the presence of oxygen-containing acidic functional groups suggested the potential for electron donation in the reduction of Cr(VI).

3.3 Mechanistic implications about CMC detoxifying

Through the assessment of intracellular ATP, GSH, and ROS concentrations, we compared the toxicity of nZVI with different stabilization methods on SL2. ATP, which is known to play a crucial role in cellular metabolism, and its concentration reflects the cellular activity (Tsitonaki et al., 2010; Wu et al., 2013). In the experimental group where only SL2 was added, the intracellular ATP content was highest, while the ATP levels significantly decreased in the groups with added materials, indicating a certain toxicity of the materials to SL2, affecting its metabolism. In comparison, the ATP content in the nZVI/CMC experimental group (0.5981 μmol/g) was higher than that in the nZVI (0.1655 μmol/g) and nZVI/C (0.2532 μmol/g) groups, suggesting that the encapsulation of CMC reduced the toxicity of nZVI to SL2.

nZVI exhibits considerable oxidative power in oxygen-containing water (Cheng et al., 2016). It can be oxidated to generate Fe(II) and H_2O_2 (Kim et al., 2011), followed by Fenton reaction to produce highly toxic ROS, such as ·OH and $\cdot O_2^-$ (Keenan and Sedlak, 2008; Xu et al., 2022). The reaction equations are as follows (Eqs 8-11):

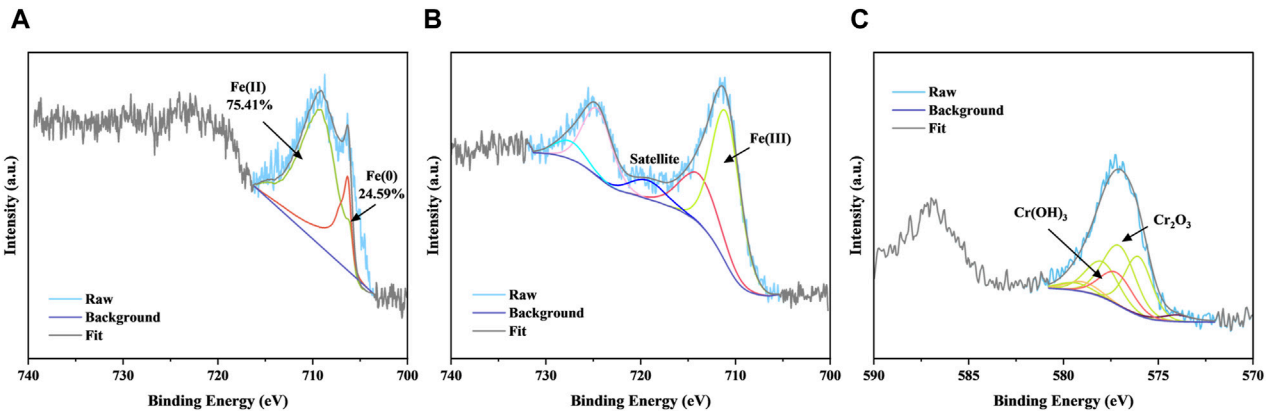

FIGURE 3
XPS spectra of Fe 2p **(A)** for fresh nZVI/CMC, Fe 2p **(B)** and Cr 2p **(C)** for product after Cr(VI) reduction. [Cr(VI)] = 200 mg/L, [nZVI/CMC] = 2 g/L, shanked at 150rpm for 24 h at 25°C.

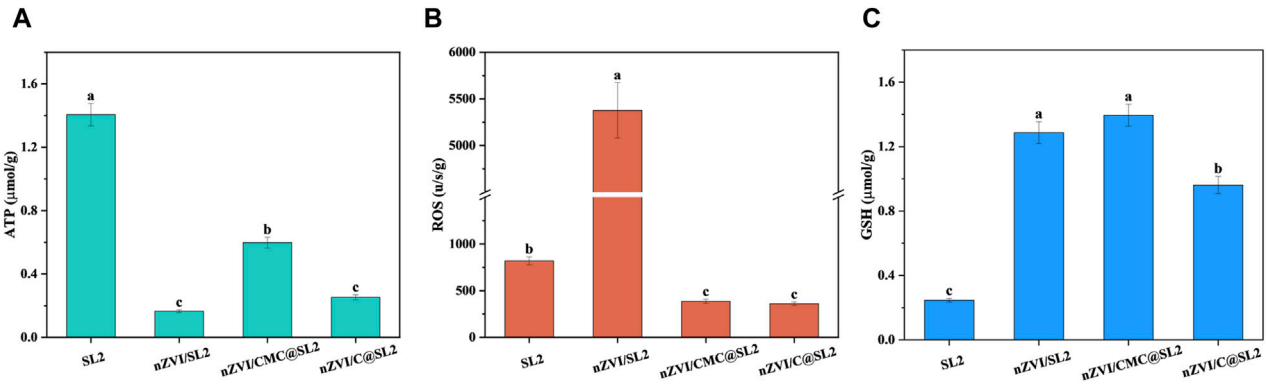

FIGURE 4
Intracellular levels of **(A)** ATP, **(B)** ROS, **(C)** GSH contents in SL2. Experimental conditions: [SL2] = 10^5 CFU/mL, [Cr(VI)] = 128 mg/L, [stabilized nZVI] = 1 g/L, 2 days.

$$Fe^0 + O_2 + 2H^+ \rightarrow Fe(II) + H_2O_2 \quad (8)$$

$$Fe^0 + H_2O_2 + 2H^+ \rightarrow Fe(II) + 2H_2O \quad (9)$$

$$Fe(II) + H_2O_2 \rightarrow Fe(III) + \cdot OH + 2OH^- \quad (10)$$

$$Fe(II) + O_2 \rightarrow Fe(III) + \cdot O_2^- \quad (11)$$

Typically, ROS produced at low frequencies are easily neutralized by antioxidant defenses (Nel et al., 2006). However, excessive ROS can overwhelm cellular antioxidant defenses, causing membrane damage (Xia et al., 2020), DNA fragmentation (Xia et al., 2019), and even cellular inactivation (Nel, 2005). Therefore, cellular oxidative stress responses were further investigated by assessing intracellular levels of ROS and GSH to elucidate the molecular mechanisms. As depicted in the Figure 4, the ROS content in the nZVI-treated group exhibited a dramatic increase (5376 u/s/g), surpassing that of other groups (819, 387 and 361 u/s/g respectively). This elevation suggested a potential dual effect: an increase in endogenous ROS production within the cells and a possible disruption of cell structures (Liu et al., 2011; Mao et al., 2019) allowing enhanced penetration of exogenous ROS (Li et al., 2022), leading to a substantial concentration surge. Simultaneously, the ROS content in the nZVI/CMC and nZVI/C remained comparatively lower, indicating a certain degree of mitigation of cellular oxidative stress reactions. From the perspective of GSH content, CMC-stabilized nZVI generated a significant amount of antioxidant enzymes to shield itself from external oxidation, thereby maintaining lower ROS levels. Although the nZVI-treated group also exhibited elevated GSH levels, it proved insufficient to eliminate the excessive intracellular ROS, resulting in an imbalance in the cellular redox state and compromising the cell's self-protective capacity.

Taken together, the results presented herein indicate a significant enhancement in surface reactivity after CMC-coating, accompanied by a concurrent reduction in the nanomaterial's toxicity towards SL2. This aligns with findings from previous studies conducted on *Escherichia coli* (Zhou et al., 2014). We hypothesize that the detoxifying effect of this CMC-coating can be attributed to three key factors: Firstly, its role as a scavenger of free radicals, leading to the substantial elimination of ·OH radicals (·OH + CMC → H_2O+ CMC*) (Joo and Zhao, 2008); Secondly, its ability to prevent direct contact between SL2 and nZVI particles (Dong et al., 2016), thereby mitigating oxidative stress reactions in

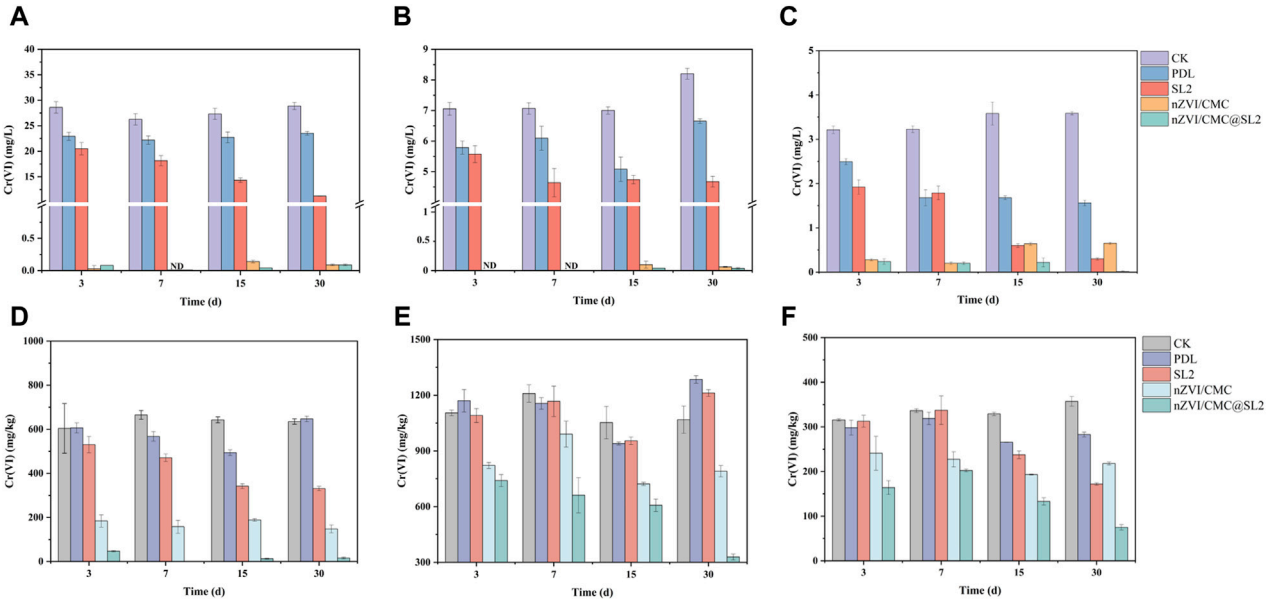

FIGURE 5
The TCLP **(A–C)** and total Cr(VI) **(D–F)** concentrations in different soils after diverse treatments, NM **(A, D)**, ZH **(B, E)**, ZL **(C, F)**.

cells and ensuring their viability; Thirdly, CMC can provide an organic carbon source for the growth of SL2 (Wang ZY. et al., 2020).

3.4 Soil remediation

In order to investigate the application potential of nZVI/CMC@SL2 in reducing Cr(VI) in soil, we conducted remediation experiments using soils from different types of contaminated sites. The TCLP method was employed to assess the leaching risk of Cr, and the changes in the total Cr(VI) content in the soil were also measured. As shown in Figure 5, after a 3-day remediation period, a significant reduction in TCLP-Cr(VI) was observed in soils amended with 0.4% nZVI/CMC. For NM, ZH, and ZL soils, the Cr(VI) concentration decreased from 28.6, 7.05, and 3.21 mg/L to less than 0.5 mg/L. However, a slight rebound was observed after 15 days, potentially attributed to the oxidation of ferrous species (Wang et al., 2023), leading to a loss of remediation capacity. Notably, the rebound was less pronounced in the presence of nZVI/CMC@SL2, indicating that the addition of SL2 could inhibit the oxidation of Cr(III). Furthermore, after 30-days remediation, the Fe(II) concentration in the nZVI/CMC@SL2 treatment group was significantly higher than in the group that only received nZVI/CMC (Figure 6). This observation indicated that SL2 could effectively facilitate the reduction of Fe(III) to Fe(II), thereby sustaining the reduction of Cr(VI). According to previous studies, oxalic acid was the most abundant LMWOA produced by strain SL2, and the affinity of oxalic acid with Cr(VI) leads to the expansion of Cr(VI) coordination from tetrahedron to hexahedron, which was preferable for hexahedral species of Cr(III). Oxalic acid was used as a substitute electron donor for Cr(VI) reduction through intramolecular electron transfer reaction, which significantly improved the Cr(VI) removal efficiency (Jiang et al., 2017). Furthermore, nZVI promoted oxalic acid secretion by SL2, and its generated iron ions could accelerate the reduction of Cr(VI) by oxalic acid (Hug et al., 1997). Studies have detected the formation of compounds containing Fe(II), Cr(V), and oxalate salts ($HCrFeC_4O_9$)(Luo et al., 2023), providing crucial evidence for the involvement of Fe(II)/Fe(III) cycling in organic acid reduction of Cr(VI). In the case of the reaction group with only SL2 added, the removal efficiency for Cr(VI) increased with prolonged incubation time within the 30-day period, suggesting that SL2 successfully colonized and persisted in the soil, continuously fixing Cr(VI) through biological processes, in accordance with SL2 biomass change (Supplementary Figure S4). For all nZVI/CMC@SL2 composite systems, the treatment groups achieved a removal efficiency of over 99.5% for TCLP-Cr(VI) after 30 days, and the TCLP-Cr(VI) was lower than the level IV standard of groundwater quality criterion in China (0.1 mg/L, GB/T 14848–2017). In addition, the total Cr(VI) in the NM soil decreased from over 600 mg/kg to 16 mg/kg, which was below the regulatory limit for Class I construction land specified in GB36600-2018 (30 mg/kg). In heavily contaminated soil (ZH, Figure 5E) with elevated concentrations of Cr(VI), the growth of SL2 was suboptimal due to the toxic effects of Cr(VI), therefore basically did not demonstrate any removal effectiveness against Cr(VI). However, with the addition of nZVI/CMC, the pollutant concentration was reduced to a level conducive to growth. This combination successfully decreased the total Cr(VI) content from around 1,200 mg/kg to approximately 300 mg/kg within a 30-day period.

This study evaluated sequential extraction procedures for identifying the relative availability of soil-bound heavy metal by partitioning the particulate trace metals into five fractions. The five species have been defined as exchangeable (F1), bound to carbonates (F2), Fe-Mn oxides-bound (F3), organic matter-bound (F4) and residual (F5). Figure 7 showed the transformation in chromium

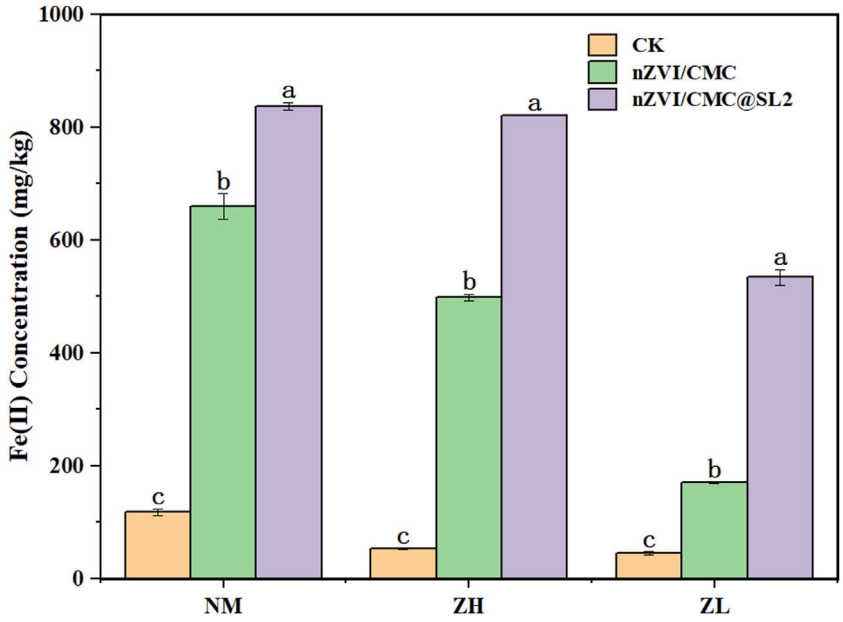

FIGURE 6
Fe(II) concentration in soil after 30-days remediation.

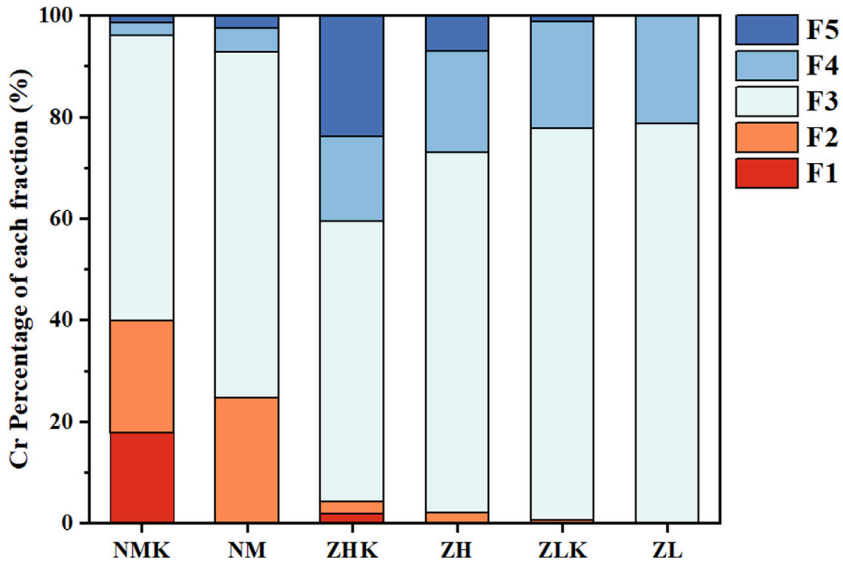

FIGURE 7
Soil Cr speciation after 30-days remediation with 0.4% nZVI/CMC@SL2. (Cr species: F1: exchangeable (EX); F2: carbonate bound (CB); F3: Fe-Mn oxide bound (OX); F4: organic matter bound (OM); F5: residual (RS); NMK and NM represented the control check and nZVI/CMC@SL2 treatment of NM soil, ZHK and ZH, ZLK and ZL were the same).

components in different treatment group which aligned with the earlier leaching results. After a 30-day treatment period, the exchangeable Cr content in all soils significantly decreased, undergoing transformation into Fe-Mn oxide-bound and the organic-bound forms. According to previous investigations, the elevated Fe-Mn oxides-bound fraction might be largely attributed to the precipitation of $Cr(OH)_3$ or Cr(III)/Fe(III) oxides/hydroxides ($Cr_nFe_{1-n}OOH$ and Cr_nFe_{1-n} $(OH)_3$) during the CMC-nZVI remediation (Manning et al., 2007). Specifically, 17.82% of exchangeable chromium in the NM soil was completely transformed into other more stable forms of Cr. According to Supplementary Figure S5, after 7 days of treatment, noticeable changes in pH were observed in the experimental groups. The group with the addition of nZVI/CMC exhibited the highest pH increase, rising from 8.70, 8.55, and 8.45 to 8.93, 8.72, and 8.70, respectively. This phenomenon may be attributed to the

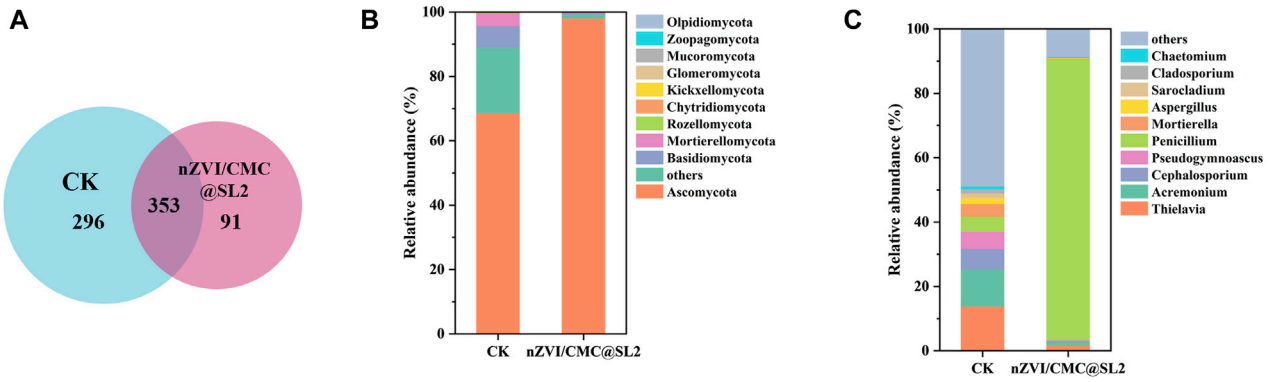

FIGURE 8
Venn diagram **(A)** based on OTU and microbial community structures (fungi) at the phylum **(B)** and genus **(C)** level of different treatments after 30-days.

alkaline nature of the material and the reduction of Cr(VI) acting in concert. In the experimental group with the addition of SL2, the pH initially showed a decline followed by an upward trend, gradually stabilizing. This suggested that SL2 proliferated extensively in the early stages, producing acidic substances, and later reached a stable state. Due to the natural buffering capacity of the complex soil system, the fluctuation range of pH during the remediation process remained relatively small.

In short, the results indicated the excellent stabilization and environmental adaptability of the nZVI/CMC@SL2 composite remediation system towards chromium. It promoted the conversion of more easily available Cr (EX and CB) to the less available (OX and OM) and thus reduce the toxic effect of Cr. Furthermore, SL2 possessed the ability to regenerate Fe(II), facilitating the sustained reduction of Cr(VI).

3.5 Microecology analysis

After 30 days of treatment, the quantity of SL2 in the nZVI/CMC@SL2 treatment group gradually stabilized and maintained at a high level (4.23×10^4 CFU/mL, Supplementary Figure S4). Microbial community analysis of the ZL soil revealed an average of 81,938 quality sequences and 740 OUTs generated from the ITS1 gene. The fungal community's similarities and differences were analyzed based on OTUs using a Venn diagram (Figure 8A). There were 353 shared OTUs, constituting 47.7% of the total observed OTUs (740), with 296 and 91 unique OUTs in the CK and treatment groups, respectively. This indicates that different treatments cultivated distinct microbial populations. Comparing with the CK, the treatment group exhibited a slight reduction in OUT levels, suggesting that this composite system could influence the fungal abundance in the soil. In terms of alpha diversity, both fungi and bacteria were significantly affected (Supplementary Table S6). In the CK group, the three most abundant fungi were *Ascomycota* (68.66%), *Basidiomycota* (6.65%), and *Mortierellomycota* (4.03%). In the experimental group, the relative abundance of *Ascomycota* surged to 98.09%. As SL2 belongs to *Ascomycota*, its relative abundance increased from 4.75% to 87.18% at genus level, further confirming the successful colonization of SL2 in the soil and its competition with indigenous microorganisms to become the dominant strain (Figure 8). Looking at the bacterial community (Supplementary Figure S6), there was a significant increase in the relative abundance of *Proteobacteria* and *Firmicutes*, rising from 38.70% to 10.68%–55.84% and 35.47%, respectively. Meanwhile, *Actinobacteria* decreased substantially (38.66%–7.35%). *Proteobacteria* was often found as a dominant species in chromium-contaminated soil (Desai et al., 2009), with *Bacillus* within this phylum known to possess Cr(VI) reductase activity, capable of resisting and reducing high concentrations of Cr(VI) (Elangovan et al., 2006; Desai et al., 2008). *Firmicutes* harbored various heavy metal resistance genes, exhibiting stronger adaptability to heavy metal-polluted environments. Also, they are reported typically to be Fe(III)-reducing bacteria (FeRB)(Jin et al., 2023), thus regenerating Fe(II) and reduce Cr(VI).

In conclusion, the nZVI/CMC@SL2 composite system enabled the successful colonization of SL2 in soils highly contaminated with Cr(VI). It demonstrates the ability to enrich chromium-tolerant and chromium-removing microorganisms, thereby promoting the reduction of Cr(VI).

4 Conclusion

In this study, nano zero-valent iron (nZVI) stabilized in different ways were successfully prepared and compared. Specifically, nZVI/CMC not only efficiently removed Cr(VI) but also exhibited a detoxification effect on SL2. The heightened reactivity towards Cr(VI) can be attributed to the smaller size of the nano particles and the abundant oxygen-containing acidic groups in CMC. The detoxification effect may result from its identity as a free radical scavenger and the direct isolation achieved through CMC-coating. Furthermore, this combination of nZVI/CMC and SL2 for the stabilization of Cr(VI) in actual contaminated site soil was successfully applied, and through multiple perspectives such as leaching risk, chemical speciation changes, and soil microecology, we revealed the composite system's application potential in soil remediation. In conclusion, the chemical-fungal composite system of nZVI/CMC@SL2 explored in this study offers a novel approach for the remediation of highly contaminated Cr(VI) site soil. However, the

mechanism by which SL2 reduces Fe(III) and the long-term stability of the nZVI/CMC@SL2 composite system remain unclear. It is recommended to delve deeper into the reduction mechanism in future research and conduct studies at field scales and real heavy metal-contaminated sites for a more comprehensive understanding.

Data availability statement

The datasets presented in this study can be found in online repositories. The names of the repository/repositories and accession number(s) can be found below: https://www.ncbi.nlm.nih.gov/bioproject/, accession number PRJNA1117622.

Author contributions

SP: Writing–review and editing, Writing–original draft, Visualization, Methodology, Investigation, Formal Analysis, Data curation, Conceptualization. JT: Writing–review and editing, Supervision, Methodology, Investigation, Formal Analysis. YL: Writing–review and editing, Methodology, Investigation, Formal Analysis. JP: Writing–review and editing, Supervision, Software. HZ: Writing–review and editing, Visualization, Resources. JW: Writing–review and editing, Visualization, Data curation. JS: Writing–review and editing, Supervision, Project administration, Funding acquisition.

Funding

The author(s) declare that financial support was received for the research, authorship, and/or publication of this article. This research was supported by the National Natural Science Foundation of China (42277004) and the National Key Research and Development Program of China (2022YFC3702104).

Acknowledgments

The authors thank the editors and reviewers for their valuable comments to improve this article.

Conflict of interest

The authors declare that the research was conducted in the absence of any commercial or financial relationships that could be construed as a potential conflict of interest.

Publisher's note

All claims expressed in this article are solely those of the authors and do not necessarily represent those of their affiliated organizations, or those of the publisher, the editors and the reviewers. Any product that may be evaluated in this article, or claim that may be made by its manufacturer, is not guaranteed or endorsed by the publisher.

Supplementary material

The Supplementary Material for this article can be found online at: https://www.frontiersin.org/articles/10.3389/fenvs.2024.1393609/full#supplementary-material

References

Ambika, S., Nambi, I. M., and Senthilnathan, J. (2016). Low temperature synthesis of highly stable and reusable CMC-Fe^{2+}(-nZVI) catalyst for the elimination of organic pollutants. *Chem. Eng. J.* 289, 544–553. doi:10.1016/j.cej.2015.12.063

Auffan, M., Achouak, W., Rose, J., Roncato, M., Chanéac, C., Waite, D. T., et al. (2008). Relation between the redox state of iron-based nanoparticles and their cytotoxicity toward *Escherichia coli*. *Environ. Sci. Technol.* 42 (17), 6730–6735. doi:10.1021/es800086f

Bai, Y., Lu, Y., Shen, N., Lau, T., and Zeng, R. J. (2018). Investigation of Cr(VI) reduction potential and mechanism by Caldicellulosiruptor saccharolyticus under glucose fermentation condition. *J. Hazard Mater* 344, 585–592. doi:10.1016/j.jhazmat.2017.10.059

Bian, H., Wan, J., Muhammad, T., Wang, G., Sang, L., Jiang, L., et al. (2021). Computational study and optimization experiment of nZVI modified by anionic and cationic polymer for Cr(VI) stabilization in soil: kinetics and response surface methodology (RSM). *Environ. Pollut.* 276, 116745. doi:10.1016/j.envpol.2021.116745

Bruins, M. R., Kapil, S., and Oehme, F. W. (2000). Microbial resistance to metals in the environment. *Ecotox Environ. Safe* 45 (3), 198–207. doi:10.1006/eesa.1999.1860

Chekli, L., Brunetti, G., Marzouk, E. R., Maoz-Shen, A., Smith, E., Naidu, R., et al. (2016). Evaluating the mobility of polymer-stabilised zero-valent iron nanoparticles and their potential to co-transport contaminants in intact soil cores. *Environ. Pollut.* 216, 636–645. doi:10.1016/j.envpol.2016.06.025

Chen, P., Tan, S., and Wu, W. (2012). Stabilization or oxidation of nanoscale zerovalent Iron at environmentally relevant exposure changes bioavailability and toxicity in medaka fish. *Environ. Sci. Technol.* 46 (15), 8431–8439. doi:10.1021/es3006783

Chen, X., Li, X., Xu, D., Yang, W., and Bai, S. (2020). Application of nanoscale zero-valent iron in hexavalent chromium-contaminated soil: a review. *A Rev.* 9 (1), 736–750. doi:10.1515/ntrev-2020-0059

Cheng, R., Li, G., Shi, L., Xue, X., Kang, M., and Zheng, X. (2016). The mechanism for bacteriophage f2 removal by nanoscale zero-valent iron. *Water Res.* 105, 429–435. doi:10.1016/j.watres.2016.09.025

Dai, Y., Zhang, K., Meng, X., Li, J., Guan, X., Sun, Q., et al. (2019). New use for spent coffee ground as an adsorbent for tetracycline removal in water. *Chemosphere* 215, 163–172. doi:10.1016/j.chemosphere.2018.09.150

Deng, J., Li, X., Wei, X., Liu, Y., Liang, J., Shao, Y., et al. (2020). Different adsorption behaviors and mechanisms of a novel amino-functionalized hydrothermal biochar for hexavalent chromium and pentavalent antimony. *Bioresour. Technol.* 310, 123438. doi:10.1016/j.biortech.2020.123438

Deng, N., Li, Z., Zuo, X., Chen, J., Shakiba, S., Louie, S. M., et al. (2021). Coprecipitation of Fe/Cr hydroxides with organics: roles of organic properties in composition and stability of the coprecipitates. *Environ. Sci. Technol.* 55 (8), 4638–4647. doi:10.1021/acs.est.0c04712

Desai, C., Jain, K., and Madamwar, D. (2008). Evaluation of *in vitro* Cr(VI) reduction potential in cytosolic extracts of three indigenous *Bacillus* sp. isolated from Cr(VI) polluted industrial landfill. *Bioresour. Technol.* 99 (14), 6059–6069. doi:10.1016/j.biortech.2007.12.046

Desai, C., Parikh, R. Y., Vaishnav, T., Shouche, Y. S., and Madamwar, D. (2009). Tracking the influence of long-term chromium pollution on soil bacterial community structures by comparative analyses of 16S rRNA gene phylotypes. *Res. Microbiol.* 160 (1), 1–9. doi:10.1016/j.resmic.2008.10.003

Dong, H., Xie, Y., Zeng, G., Tang, L., Liang, J., He, Q., et al. (2016). The dual effects of carboxymethyl cellulose on the colloidal stability and toxicity of nanoscale zero-valent iron. *Chemosphere* 144, 1682–1689. doi:10.1016/j.chemosphere.2015.10.066

Du, H., Li, N., Yang, L., Li, Q., Yang, G., and Wang, Q. (2023). Plasmonic Ag modified Ag_3VO_4/AgPMo S-scheme heterojunction photocatalyst for boosted Cr(VI) reduction

under visible light: performance and mechanism. *Sep. Purif. Technol.* 304, 122204. doi:10.1016/j.seppur.2022.122204

Edgar, R. C. (2013). UPARSE: highly accurate OTU sequences from microbial amplicon reads. *Nat. Methods* 10 (10), 996–998. doi:10.1038/nmeth.2604

Elangovan, R., Abhipsa, S., Rohit, B., Ligy, P., and Chandraraj, K. (2006). Reduction of Cr(VI) by a *Bacillus* sp. *Biotechnol. Lett.* 28 (4), 247–252. doi:10.1007/s10529-005-5526-z

Fang, Z., Qiu, X., Huang, R., Qiu, X., and Li, M. (2011). Removal of chromium in electroplating wastewater by nanoscale zero-valent metal with synergistic effect of reduction and immobilization. *Desalination* 280 (1), 224–231. doi:10.1016/j.desal.2011.07.011

Fu, Y., Xu, Y., Mao, Y., Tan, M., He, Q., Mao, H., et al. (2023). Multi-functional Ag/Ag_3PO_4/AgPMo with S-scheme heterojunction for boosted photocatalytic performance. *Sep. Purif. Technol.* 317, 123922. doi:10.1016/j.seppur.2023.123922

Gong, Y., Gai, L., Tang, J., Fu, J., Wang, Q., and Zeng, E. Y. (2017). Reduction of Cr(VI) in simulated groundwater by FeS-coated iron magnetic nanoparticles. *Sci. Total Environ.* 595, 743–751. doi:10.1016/j.scitotenv.2017.03.282

He, F., and Zhao, D. (2007). Manipulating the size and dispersibility of zerovalent iron nanoparticles by use of carboxymethyl cellulose stabilizers. *Environ. Sci. Technol.* 41 (17), 6216–6221. doi:10.1021/es0705543

He, F., Zhao, D., Liu, J., and Roberts, C. B. (2007). Stabilization of Fe–Pd nanoparticles with sodium carboxymethyl cellulose for enhanced transport and dechlorination of trichloroethylene in soil and groundwater. *Ind. Eng. Chem. Res.* 46 (1), 29–34. doi:10.1021/ie0610896

Hou, S., Wu, B., Luo, Y., Li, Y., Ma, H., Peng, D., et al. (2020). Impacts of a novel strain QY-1 allied with chromium immobilizing materials on chromium availability and soil biochemical properties. *J. Hazard Mater* 382, 121093. doi:10.1016/j.jhazmat.2019.121093

Hug, S. J., Laubscher, H., and James, B. R. (1997). Iron(III) catalyzed photochemical reduction of chromium(VI) by oxalate and citrate in aqueous solutions. *Environ. Sci. Technol.* 31 (1), 160–170. doi:10.1021/es960253l

Ji, X., Wan, J., Wang, X., Peng, C., Wang, G., Liang, W., et al. (2022). Mixed bacteria-loaded biochar for the immobilization of arsenic, lead, and cadmium in a polluted soil system: effects and mechanisms. *Sci. Total Environ.* 811, 152112. doi:10.1016/j.scitotenv.2021.152112

Jiang, B., Xin, S., Gao, L., Luo, S., Xue, J., and Wu, M. (2017). Dramatically enhanced aerobic Cr(VI) reduction with scrap zero-valent aluminum induced by oxalate. *Chem. Eng. J.* 308, 588–596. doi:10.1016/j.cej.2016.09.098

Jin, Y., Wang, Y., Li, X., Luo, T., Ma, Y., Wang, B., et al. (2023). Remediation and its biological responses to Cd(II)-Cr(VI)-Pb(II) multi-contaminated soil by supported nano zero-valent iron composites. *Sci. Total Environ.* 867, 161344. doi:10.1016/j.scitotenv.2022.161344

Joo, S. H., and Zhao, D. (2008). Destruction of lindane and atrazine using stabilized iron nanoparticles under aerobic and anaerobic conditions: effects of catalyst and stabilizer. *Chemosphere* 70 (3), 418–425. doi:10.1016/j.chemosphere.2007.06.070

Keenan, C. R., and Sedlak, D. L. (2008). Factors affecting the yield of oxidants from the reaction of nanoparticulate zero-valent iron and oxygen. *Environ. Sci. Technol.* 42 (4), 1262–1267. doi:10.1021/es7025664

Kim, J. Y., Lee, C., Love, D. C., Sedlak, D. L., Yoon, J., and Nelson, K. L. (2011). Inactivation of MS2 coliphage by ferrous ion and zero-valent iron nanoparticles. *Environ. Sci. Technol.* 45 (16), 6978–6984. doi:10.1021/es201345y

Laumann, S., Micić, V., and Hofmann, T. (2014). Mobility enhancement of nanoscale zero-valent iron in carbonate porous media through co-injection of polyelectrolytes. *Water Res.* 50, 70–79. doi:10.1016/j.watres.2013.11.040

Li, L., Dong, H., Lu, Y., Zhang, H., Li, Y., Xiao, J., et al. (2022). In-depth exploration of toxicity mechanism of nanoscale zero-valent iron and its aging products toward *Escherichia coli* under aerobic and anaerobic conditions. *Environ. Pollut.* 313, 120118. doi:10.1016/j.envpol.2022.120118

Li, Y., Pan, S., Wang, L., Jia, F., Lu, F., and Shi, J. (2023). Soil chromium accumulation in Industrial regions across China: pollution and health risk assessment, spatial pattern, and temporal trend (2002-2021). *Toxics* 11, 363. doi:10.3390/toxics11040363

Lin, W., Chen, C., Ou, J., Sheu, Y., Hou, D., and Kao, C. (2022). Bioremediation of hexavalent-chromium contaminated groundwater: microcosm, column, and microbial diversity studies. *Chemosphere* 295, 133877. doi:10.1016/j.chemosphere.2022.133877

Lin, Y., Tseng, H., Wey, M., and Lin, M. (2010). Characteristics of two types of stabilized nano zero-valent iron and transport in porous media. *Sci. Total Environ.* 408 (10), 2260–2267. doi:10.1016/j.scitotenv.2010.01.039

Liu, K., Li, F., Cui, J., Yang, S., and Fang, L. (2020). Simultaneous removal of Cd(II) and As(III) by graphene-like biochar-supported zero-valent iron from irrigation waters under aerobic conditions: synergistic effects and mechanisms. *J. Hazard Mater* 395, 122623. doi:10.1016/j.jhazmat.2020.122623

Liu, S., Zeng, T. H., Hofmann, M., Burcombe, E., Wei, J., Jiang, R., et al. (2011). Antibacterial activity of graphite, graphite oxide, graphene oxide, and reduced graphene oxide: membrane and oxidative stress. *Acs Nano* 5 (9), 6971–6980. doi:10.1021/nn202451x

Liu, T., Zhao, L., Sun, D., and Tan, X. (2010). Entrapment of nanoscale zero-valent iron in chitosan beads for hexavalent chromium removal from wastewater. *J. Hazard Mater* 184 (1), 724–730. doi:10.1016/j.jhazmat.2010.08.099

Long, B., Liao, L., Jia, F., Luo, Y., He, J., Zhang, W., et al. (2023). Oxalic acid enhances bioremediation of Cr(VI) contaminated soil using *Penicillium oxalicum* SL2. *Chemosphere* 311, 136973. doi:10.1016/j.chemosphere.2022.136973

Long, B., Ye, B., Liu, Q., Zhang, S., Ye, J., Zou, L., et al. (2018). Characterization of *Penicillium oxalicum* SL2 isolated from indoor air and its application to the removal of hexavalent chromium. *Plos One* 13 (1), e0191484. doi:10.1371/journal.pone.0191484

Luo, Y., Pang, J., Peng, C., Ye, J., Long, B., Tong, J., et al. (2023). Cr(VI) reduction and Fe(II) regeneration by *Penicillium oxalicum* SL2-enhanced nanoscale zero-valent iron. *Environ. Sci. Technol.* 57 (30), 11313–11324. doi:10.1021/acs.est.3c01390

Lyu, H., Tang, J., Huang, Y., Gai, L., Zeng, E. Y., Liber, K., et al. (2017). Removal of hexavalent chromium from aqueous solutions by a novel biochar supported nanoscale iron sulfide composite. *Chem. Eng. J.* 322, 516–524. doi:10.1016/j.cej.2017.04.058

Ma, L., Du, Y., Chen, S., Zhang, F., Zhan, W., Du, D., et al. (2021). Nanoscale zero-valent iron coupling with Shewanella oneidensis MR-1 for enhanced reduction/removal of aqueous Cr(VI). *Sep. Purif. Technol.* 277, 119488. doi:10.1016/j.seppur.2021.119488

Ma, X., Du, H., Tan, M., Qian, J., Deng, M., Hao, D., et al. (2024). Photocatalytic fuel cell with cathodic P-$BiVO_4$/CQDs and anodic WO_3 for efficient Cr(VI) reduction and stable electricity generation. *Sep. Purif. Technol.* 339, 126644. doi:10.1016/j.seppur.2024.126644

Manning, B. A., Kiser, J. R., Kwon, H., and Kanel, S. R. (2007). Spectroscopic investigation of Cr(III)- and Cr(VI)-treated nanoscale zerovalent iron. *Environ. Sci. Technol.* 41 (2), 586–592. doi:10.1021/es061721m

Mao, C., Xiang, Y., Liu, X., Zheng, Y., Yeung, K. W. K., Cui, Z., et al. (2019). Local photothermal/photodynamic synergistic therapy by disrupting bacterial membrane to accelerate reactive oxygen species permeation and protein leakage. *Acs Appl. Mater Inter* 11 (19), 17902–17914. doi:10.1021/acsami.9b05787

Megharaj, M., Avudainayagam, S., and Naidu, R. (2003). Toxicity of hexavalent chromium and its reduction by bacteria isolated from soil contaminated with tannery waste. *Curr. Microbiol.* 47 (1), 51–54. doi:10.1007/s00284-002-3889-0

Morales, D. K., Ocampo, W., and Zambrano, M. M. (2007). Efficient removal of hexavalent chromium by a tolerant *Streptomyces* sp. affected by the toxic effect of metal exposure. *J. Appl. Microbiol.* 103 (6), 2704–2712. doi:10.1111/j.1365-2672.2007.03510.x

Nel, A. (2005). Air pollution-related illness: effects of particles. *Science* 308 (5723), 804–806. doi:10.1126/science.1108752

Nel, A., Xia, T., Mädler, L., and Li, N. (2006). Toxic potential of materials at the nanolevel. *Science* 311 (5761), 622–627. doi:10.1126/science.1114397

Pan, C., Troyer, L. D., Catalano, J. G., and Giammar, D. E. (2016). Dynamics of chromium(VI) removal from drinking water by iron electrocoagulation. *Environ. Sci. Technol.* 50 (24), 13502–13510. doi:10.1021/acs.est.6b03637

Peng, L., Liu, Y., Gao, S., Dai, X., and Ni, B. (2015). Assessing chromate reduction by dissimilatory iron reducing bacteria using mathematical modeling. *Chemosphere* 139, 334–339. doi:10.1016/j.chemosphere.2015.06.090

Phenrat, T., Saleh, N., Sirk, K., Tilton, R. D., and Lowry, G. V. (2007). Aggregation and sedimentation of aqueous nanoscale zerovalent iron dispersions. *Environ. Sci. Technol.* 41 (1), 284–290. doi:10.1021/es061349a

Qian, A., Liao, P., Yuan, S., and Luo, M. (2014). Efficient reduction of Cr(VI) in groundwater by a hybrid electro-Pd process. *Water Res.* 48, 326–334. doi:10.1016/j.watres.2013.09.043

Qu, J., Wang, Y., Tian, X., Jiang, Z., Deng, F., Tao, Y., et al. (2021). KOH-activated porous biochar with high specific surface area for adsorptive removal of chromium (VI) and naphthalene from water: affecting factors, mechanisms and reusability exploration. *J. Hazard Mater* 401, 123292. doi:10.1016/j.jhazmat.2020.123292

Qu, J., Wei, S., Liu, Y., Zhang, X., Jiang, Z., Tao, Y., et al. (2022). Effective lead passivation in soil by bone char/CMC-stabilized FeS composite loading with phosphate-solubilizing bacteria. *J. Hazard Mater* 423, 127043. doi:10.1016/j.jhazmat.2021.127043

Rajapaksha, A. U., Alam, M. S., Chen, N., Alessi, D. S., Igalavithana, A. D., Tsang, D. C. W., et al. (2018). Removal of hexavalent chromium in aqueous solutions using biochar: chemical and spectroscopic investigations. *Sci. Total Environ.* 625, 1567–1573. doi:10.1016/j.scitotenv.2017.12.195

Raychoudhury, T., Tufenkji, N., and Ghoshal, S. (2012). Aggregation and deposition kinetics of carboxymethyl cellulose-modified zero-valent iron nanoparticles in porous media. *Water Res.* 46 (6), 1735–1744. doi:10.1016/j.watres.2011.12.045

Ren, L., Dong, J., Chi, Z., and Huang, H. (2018). Reduced graphene oxide-nano zero value iron (rGO-nZVI) micro-electrolysis accelerating Cr(VI) removal in aquifer. *J. Environ. Sci-China* 73, 96–106. doi:10.1016/j.jes.2018.01.018

Su, C., and Puls, R. W. (2004). Nitrate reduction by zerovalent iron: effects of formate, oxalate, citrate, chloride, sulfate, borate, and phosphate. *Environ. Sci. Technol.* 38 (9), 2715–2720. doi:10.1021/es034650p

Su, H., Fang, Z., Tsang, P. E., Zheng, L., Cheng, W., Fang, J., et al. (2016). Remediation of hexavalent chromium contaminated soil by biochar-supported zero-valent iron nanoparticles. *J. Hazard Mater* 318, 533–540. doi:10.1016/j.jhazmat.2016.07.039

Sun, J., Luo, Y., Ye, J., Li, C., and Shi, J. (2022). Chromium distribution, leachability and speciation in a chrome plating site. *Processes* 10, 142. doi:10.3390/pr10010142

Tan, H., Wang, C., Li, H., Peng, D., Zeng, C., and Xu, H. (2020). Remediation of hexavalent chromium contaminated soil by nano-FeS coated humic acid complex in combination with Cr-resistant microflora. *Chemosphere* 242, 125251. doi:10.1016/j.chemosphere.2019.125251

Tang, J., Huang, Y., Gong, Y., Lyu, H., Wang, Q., and Ma, J. (2016). Preparation of a novel graphene oxide/Fe-Mn composite and its application for aqueous Hg(II) removal. *J. Hazard Mater* 316, 151–158. doi:10.1016/j.jhazmat.2016.05.028

Tang, X., Liu, B., Deng, Q., Zhang, R., Li, X., and Xu, H. (2018). Strengthening detoxication impacts of Coprinus comatus on nickel and fluoranthene co-contaminated soil by bacterial inoculation. *J. Environ. Manage* 206, 633–641. doi:10.1016/j.jenvman.2017.11.009

Tong, J., Ye, B., Jiang, X., Wu, H., Xu, Q., Luo, Y., et al. (2023). Synergy among extracellular adsorption, bio-precipitation and transmembrane transport of *Penicillium oxalicum* SL2 enhanced Pb stabilization. *J. Hazard Mater* 454, 131537. doi:10.1016/j.jhazmat.2023.131537

Tsitonaki, A., Petri, B., Crimi, M., Mosbek, H., Siegrist, R., and Bjerg, P. (2010). *In situ* chemical oxidation of contaminated soil and groundwater using persulfate: a review. *Crit. Rev. Env. Sci. Tec.* 40 (1), 55–91. doi:10.1080/10643380802039303

Wang, K., Sun, Y., Tang, J., He, J., and Sun, H. (2020a). Aqueous Cr(VI) removal by a novel ball milled Fe0-biochar composite: role of biochar electron transfer capacity under high pyrolysis temperature. *Chemosphere* 241, 125044. doi:10.1016/j.chemosphere.2019.125044

Wang, L., Luo, Y., Pang, J., Li, Y., Wu, H., Jiang, X., et al. (2023). Fe-biochar for simultaneous stabilization of chromium and arsenic in soil: rational design and long-term performance. *Sci. Total Environ.* 862, 160843. doi:10.1016/j.scitotenv.2022.160843

Wang, Q., Ma, W., Qian, J., Li, N., Zhang, C., Deng, M., et al. (2024). S-scheme towards interfacial charge transfer between POMs and MOFs for efficient visible-light photocatalytic Cr (VI) reduction. *Environ. Pollut.* 347, 123707. doi:10.1016/j.envpol.2024.123707

Wang, Y., Fang, Z., Kang, Y., and Tsang, E. P. (2014). Immobilization and phytotoxicity of chromium in contaminated soil remediated by CMC-stabilized nZVI. *J. Hazard Mater* 275, 230–237. doi:10.1016/j.jhazmat.2014.04.056

Wang, Z. Y., Wang, R. X., Zhou, J. S., Cheng, J. F., and Li, Y. H. (2020b). An assessment of the genomics, comparative genomics and cellulose degradation potential of Mucilaginibacter polytrichastri strain RG4-7. *Bioresour. Technol.* 297, 122389. doi:10.1016/j.biortech.2019.122389

Wu, D., Shen, Y., Ding, A., Mahmood, Q., Liu, S., and Tu, Q. (2013). Effects of nanoscale zero-valent iron particles on biological nitrogen and phosphorus removal and microorganisms in activated sludge. *J. Hazard Mater* 262, 649–655. doi:10.1016/j.jhazmat.2013.09.038

Wu, W., Wu, P., Yang, F., Sun, D., Zhang, D., and Zhou, Y. (2018). Assessment of heavy metal pollution and human health risks in urban soils around an electronics manufacturing facility. *Sci. Total Environ.* 630, 53–61. doi:10.1016/j.scitotenv.2018.02.183

Xia, D., Liu, H., Xu, B., Wang, Y., Liao, Y., Huang, Y., et al. (2019). Single Ag atom engineered 3D-MnO_2 porous hollow microspheres for rapid photothermocatalytic inactivation of *E. coli* under solar light. *Appl. Catal. B Environ.* 245, 177–189. doi:10.1016/j.apcatb.2018.12.056

Xia, D., Tang, Z., Wang, Y., Yin, R., He, H., Xie, X., et al. (2020). Piezo-catalytic persulfate activation system for water advanced disinfection: process efficiency and inactivation mechanisms. *Chem. Eng. J.* 400, 125894. doi:10.1016/j.cej.2020.125894

Xu, X., Huang, H., Zhang, Y., Xu, Z., and Cao, X. (2019). Biochar as both electron donor and electron shuttle for the reduction transformation of Cr(VI) during its sorption. *Environ. Pollut.* 244, 423–430. doi:10.1016/j.envpol.2018.10.068

Xu, Z., Wan, Z., Sun, Y., Gao, B., Hou, D., Cao, X., et al. (2022). Electroactive Fe-biochar for redox-related remediation of arsenic and chromium: distinct redox nature with varying iron/carbon speciation. *J. Hazard Mater* 430, 128479. doi:10.1016/j.jhazmat.2022.128479

Xu, Z., Xu, X., Tsang, D. C. W., Yang, F., Zhao, L., Qiu, H., et al. (2020). Participation of soil active components in the reduction of Cr(VI) by biochar: differing effects of iron mineral alone and its combination with organic acid. *J. Hazard Mater* 384, 121455. doi:10.1016/j.jhazmat.2019.121455

Yamashita, T., and Hayes, P. (2008). Analysis of XPS spectra of Fe^{2+} and Fe^{3+} ions in oxide materials. *Appl. Surf. Sci.* 254 (8), 2441–2449. doi:10.1016/j.apsusc.2007.09.063

Yang, Z., Zhang, X., Jiang, Z., Li, Q., Huang, P., Zheng, C., et al. (2021). Reductive materials for remediation of hexavalent chromium contaminated soil – a review. *Sci. Total Environ.* 773, 145654. doi:10.1016/j.scitotenv.2021.145654

Yao, Q., Liu, J., Yu, Z., Li, Y., Jin, J., Liu, X., et al. (2017). Three years of biochar amendment alters soil physiochemical properties and fungal community composition in a black soil of northeast China. *Soil Biol. Biochem.* 110, 56–67. doi:10.1016/j.soilbio.2017.03.005

Ye, J., Luo, Y., Sun, J., and Shi, J. (2021). Nanoscale zero-valent iron modified by bentonite with enhanced Cr(VI) removal efficiency, improved mobility, and reduced toxicity. *Nanomaterials* 11, 2580. doi:10.3390/nano11102580

Zhang, S., Lyu, H., Tang, J., Song, B., Zhen, M., and Liu, X. (2019). A novel biochar supported CMC stabilized nano zero-valent iron composite for hexavalent chromium removal from water. *Chemosphere* 217, 686–694. doi:10.1016/j.chemosphere.2018.11.040

Zhao, N., Tan, X., Xiong, J., Chen, N., Gao, J., Wang, R., et al. (2022). Quantitative analysis on the redox conversion mechanism of Cr(VI) and As(III) by iron carbide based biochar composites. *Chem. Eng. J.* 446, 137417. doi:10.1016/j.cej.2022.137417

Zhou, H., Ma, M., Zhao, Y., Baig, S. A., Hu, S., Ye, M., et al. (2022). Integrated green complexing agent and biochar modified nano zero-valent iron for hexavalent chromium removal: a characterisation and performance study. *Sci. Total Environ.* 834, 155080. doi:10.1016/j.scitotenv.2022.155080

Zhou, L., Thanh, T. L., Gong, J., Kim, J., Kim, E., and Chang, Y. (2014). Carboxymethyl cellulose coating decreases toxicity and oxidizing capacity of nanoscale zerovalent iron. *Chemosphere* 104, 155–161. doi:10.1016/j.chemosphere.2013.10.085

Zhu, H., Jiang, R., Xiao, L., and Li, W. (2010). A novel magnetically separable γ-Fe_2O_3/crosslinked chitosan adsorbent: preparation, characterization and adsorption application for removal of hazardous azo dye. *J. Hazard Mater* 179 (1), 251–257. doi:10.1016/j.jhazmat.2010.02.087